OPEN ACCESS

University of BRISTOL

Peer reviewed version

Link to published version (if available):
10.1021/acs.analchem.6b01659

Link to publication record in Explore Bristol Research
PDF-document

University of Bristol - Explore Bristol Research
General rights

Laser Ablation – Accelerator Mass Spectrometry: a novel approach for rapid radiocarbon analyses of carbonate archives at high spatial resolution

Caroline Welte[1,2], Lukas Wacker[2], Bodo Hattendorf[1], Marcus Christl[2], Christiane Yeman[2], Jens Fohlmeister[3], Sebastian F.M. Breitenbach[4], Laura F. Robinson[5], Allen H. Andrews[6], André Freiwald[7], Jesse R. Farmer[8], Hans-Arno Synal[2], Detlef Günther[1]

[1] Laboratory of Inorganic Chemistry, D-CHAB, ETHZ, Vladimir-Prelog Weg 1, 8093 Zurich, Switzerland

[2] Laboratory of Ion Beam Physics, ETHZ, Otto-Stern Weg 5, HPK, 8093 Zurich, Switzerland

[3] Institute for Environmental Physics, University of Heidelberg, Germany

[4]Institute of Geology, Mineralogy and Geophysics, Ruhr-University Bochum, Bochum, Germany

[5] School of Earth Sciences, University of Bristol, UK

[6] NOAA Fisheries, Pacific Islands Fisheries Science Center, USA

[7] Senckenberg am Meer, Abteilung Meeresforschung, Wilhelmshaven, Germany

[8] Earth and Environmental Sciences and Lamont-Doherty Earth Observatory of Columbia University, New York, USA

Abstract

A new instrumental setup, combining laser ablation (LA) with accelerator mass spectrometry (AMS), has been investigated for the online radiocarbon (^{14}C) analysis of carbonate records. Samples were placed in an in-house designed LA-cell and CO_2 gas was produced by ablation using a 193 nm ArF excimer laser. The ^{14}C/^{12}C abundance ratio of the gas was then analyzed by gas ion source AMS. This configuration allows flexible and time resolved acquisition of ^{14}C profiles in contrast to conventional measurements, where only the bulk composition of discrete samples can be obtained. Three different measurement modes, i.e. discrete layer analysis, survey scans and precision scans, were investigated and compared using a

28 stalagmite sample and, subsequently, applied to terrestrial and marine carbonates. Depending on the

29 measurement mode, a precision of typically 1-5 % combined with a spatial resolution of 100 µm can be

30 obtained. Prominent ^{14}C features, such as the atomic bomb ^{14}C peak, can be resolved by scanning several

31 cm of a sample within one hour. Stalagmite, deep-sea coral and mollusk shell samples yielded comparable

32 signal intensities, which again were comparable to those of conventional gas measurements. The novel

33 LA-AMS setup allowed rapid scans on a variety of sample materials with high spatial resolution.

1. Introduction

35 Carbonate radiocarbon (^{14}C) records are of great interest in a variety of research fields, such as

36 paleoclimatology[1,2], establishing or improving chronologies[3-5] understanding the carbon cycle[6,7], and age

37 validation of marine organisms[8]. Because carbonates usually can be radiometrically dated (e.g., Uranium-

38 Thorium (U/Th) disequilibrium methods[9,10]), ^{14}C in stalagmites and corals provides a powerful geochemical

39 tracer to study, for example for soil carbon dynamics[11-13] and/or past ocean circulation[14,15]. In very young

40 carbonates (<200 years) where U/Th dating becomes less precise, the detection of the atomic bomb [14]C

41 peak caused by nuclear weapon tests during the 1950s and 1960s may provide indirect, stratigraphic age

42 information[16,17]. Either of the above applications requires access to the ^{14}C signature along the archive's

43 growth axis at high spatial resolution, which involves the analysis of a great quantity of small subsamples.

44 Micro-sampling for conventional ^{14}C analysis is commonly done by micromilling techniques, reaching

45 spatial resolutions of a few dozen to hundreds of µm, but requiring an enormous work load [11,13,18]. In

46 addition to the tedious sampling process, the following multi-step chemical procedure (including

47 graphitization) necessary for the ^{14}C analysis by accelerator mass spectrometry (AMS) involves the risk of

48 sample contamination.

49 The coupling of laser ablation (LA) with inductively coupled plasma mass spectrometry (LA-ICPMS) is a

50 widely used analytical technique that allows rapid analyses of solid materials at high spatial resolution,

51 while little to no sample preparation is required[19-21]. To date, LA has mainly been applied to elemental and

52 isotopic analyses of solid materials, and there are few studies that deal with ^{14}C measurements where LA

53 is used as a sampling technique. Rosenheim, et al. [22] showed that when focusing a UV laser (quintupled

54 Nd:YAG, 213 nm) onto a carbonate sample, approximately 30 % of the ablated material was converted

55 into CO_2. In this pilot study, the CO_2 was converted into graphite for a conventional accelerator mass

56 spectrometry (AMS) measurement and therefore it did not benefit from the online injection of CO_2 when

57 using gas ion source AMS[23,24]. Fractionation effects that may occur during the ablation event and might

58 lead to fractionation of the C isotopes are not of concern in AMS analyses, as the internal normalization

59   using the $^{13}C/^{12}C$ ratio should also correct for mass dependent fractionation effects that occur during

60   ablation. Wacker, et al. [25] performed the first direct coupling of LA with AMS using a commercial LA unit

61   (LSX 213, CETAC Technologies, Omaha, USA) and a simple LA-cell design. In the proof of principle

62   experiment they performed, the known $^{14}C/^{12}C$ ratio of a natural sample was reproduced within

63   uncertainty. Subsequently, an LA-setup with optimized cell geometry was designed[26,27]. This novel LA-AMS

64   setup offers high flexibility regarding analysis time, spatial resolution and measurement precision.

65   Standards were reproduced within uncertainties and the blank level allows ^{14}C-measurements to ages as

66   old as 35 000 years.

67   The aim of this study was to demonstrate the applicability of the novel LA-AMS setup in the analysis of

68   natural carbonate samples. First, different laser scanning modes implemented into the new setup were

69   compared with regard to analysis time, material consumption, spatial resolution and measurement

70   precision. Second, the applicability of the system to different materials such as stalagmites, corals and

71   shells was investigated and $^{14}C/^{12}C$ data from conventional graphite AMS analysis could be reproduced

72   within the uncertainties using LA-AMS.

73

2. Methods

2.1.Instrumental Setup

An ArF excimer laser (Ex5, Argon Fluoride 193 nm, GAM LASER, Orlando, USA) operating at a wavelength of 193 nm is used to generate pulses at a repetition rate ranging from 150 - 250 Hz and a fluence between 1 and 2.5 J/cm^2 on the sample surface, delivered as a rectangular spot of 110 x 680 µm^2. The ablation process can be observed via a monochrome CCD camera (AVT MANTA G-125B, Allied Vision Technologies, Stadtroda, Germany) combined with a zoom lens (OPTO TUBUS Z-1,0/146, Opto, Gräfelfing, Germany). The ablation rate of the LA-AMS system is approximately 100 µg/min of $CaCO_3$ when ablating at a laser repetition rate of 200 Hz. Samples with maximum dimensions of 150 x 25 x 15 mm^3 can be placed in the sample holder of an in-house designed LA-cell (Figure 1, adapted from [27]), which is equipped with a xy-positioning system (SLC, SmarAct GmbH, Germany) that allows precise positioning of the sample relative to the laser beam. Helium is used as a carrier gas to transport the laser-produced CO_2 from the ablation spot to the ion source via a fused silica capillary ("5" in Figure 1). The background helium pressure in the LA-cell was adjusted to provide a gas flow rate on the order of 1.5 mL/min through the capillary. A detailed description of the LA-cell and the gas handling system can be found in [27].

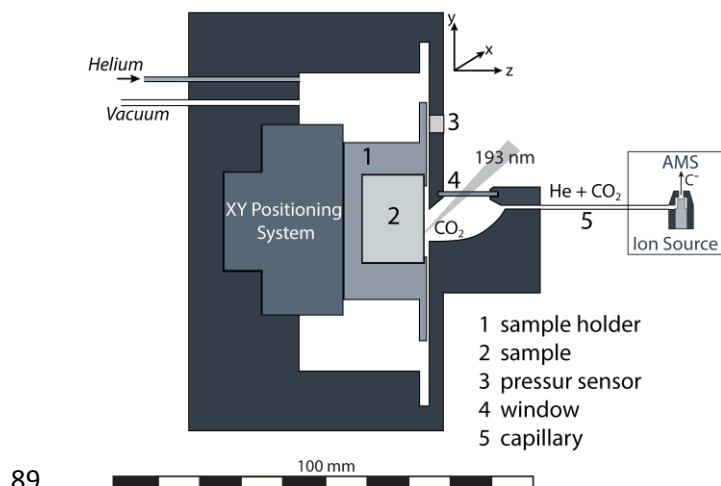

Figure 1 Schematic of the LA-AMS setup: CO$_2$ is produced in the ablation cell by focusing an ArF laser operating at 193 nm on the carbonate sample. The CO$_2$ is transported with helium as carrier gas into the gas ion source of the AMS, where negative C ions are formed and the ^{14}C content is measured.

The ^{14}C-measurements were performed with the ETH Zurich MIniCArbonDAtingSystem AMS system[28,29] (MICADAS, Ionplus AG, Dietikon, Switzerland) that is routinely used for gas measurements[23,24]. Prior to LA-AMS measurements the AMS was optimized for highest sensitivity by direct injection of a 5 % CO$_2$ in helium gas mixture. Subsequently, two to three conventional gas standards (NIST Ox-I or NIST Ox-II) and two to

three conventional ^{14}C blanks (5 % CO_2 in helium, Messer Schweiz AG, Lenzburg, Switzerland) were measured to ensure optimum working conditions of the MICADAS. A blank and fractionation correction was applied to the measured $^{14}C/^{12}C$-ratios and, subsequently, normalization to the calibration standard was performed using the data evaluation software BATS[30]. The final data are reported as $F^{14}C$ (fraction modern), which corresponds to the activity ratio of the sample relative to a modern reference material[10,31]. Initially, conventional OxI and OxII gas standards were used for calibration of the samples because no suitable solid standard material was available. Subsequently, a homogenized and compacted carbonate powder from a coral (CSTD)[32] with a nominal $F^{14}C$ of 0.9445 ± 0.0018 was measured before and after each sample analysis and used for normalization. Details on the standards used for normalization can be found in Table 1.

2.2. Modes of measurement

Requiring only minimal sample preparation (compare [27]), the LA-AMS setup provides discrete data with a minimum integration time of 10 sec. The XY-positioning system in the LA-cell was controlled by an in-house implemented LabVIEW program (National Instruments, Austin, Texas, USA) and allowed precise movement of the sample relative to the laser beam. Three contrasting sampling strategies (Modes 1-3) were developed in order to provide flexibility in adapting to the analysis purpose and the required precision (Figure 2).
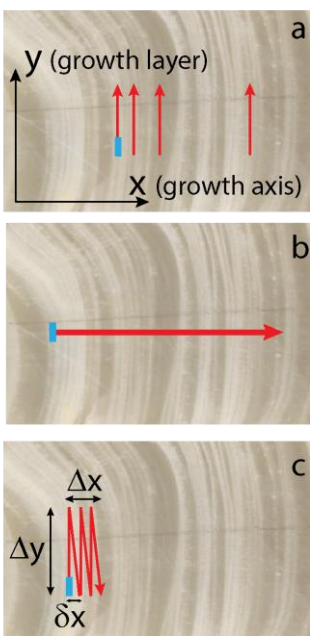
1) **Discrete layer analyses (Mode 1, Figure 2a)** are equivalent to conventional drilling of samples by ablating material parallel to individual growth layers only (i.e. within carbonate deposits that formed at the same time). The spatial resolution along the growth axis depends on the laser beam width (i.e., 110 µm).

2) A **survey scan (Mode 2, Figure 2b)** allows scanning along a sample parallel to the growth direction. The spatial resolution depends on laser beam size, laser repetition rate and scan speed.

3) **Precision scan (Mode 3, Figure 2c)** aims for continuous sampling along the growth axis, while the sampling time within the growth layer is increased by scanning in a zig-zag pattern. Part of the scan (Δy) is performed within single growth layers, followed by a return scan with a displacement δx along the x-axis. The entire scan length along the growth axis will be denoted as Δx. In the following the parameters are reported as (Δx, Δy, δx).

128

Figure 2 *Comparison of the three scanning modes available for LA-AMS measurements. (a) Mode 1: Discrete layer analysis within discrete growth layers, (b) Mode 2: Survey scans parallel to the growth direction, (c) Mode 3: Precision scans. The red arrows represent the scanning direction and the blue rectangle indicates the orientation of the laser spot.*

129

130 In the case of conventional ^{14}C AMS measurements, data evaluation had the following scheme: individual

131 samples were measured and the normalized ^{14}C/^{12}C-ratios were integrated yielding one averaged ^{14}C/^{12}C

132 ratio per sample. Hence, the data integration period was equal to the data acquisition period, which was

133 also the case for Mode 1 in LA-AMS analysis. Modes 2 and 3 required a different data evaluation

134 procedure: the ^{14}C/^{12}C-ratio continuously changes as the laser scans across different growth layers of the

135 carbonate record and depending on the measurement time one or more sputter targets of the gas ion

136 source were used. This offered the greatest flexibility concerning data evaluation, such as the data

137 integration periods; hence, spatial resolution and measurement precision could be selected according to

138 the needs of the application after the analysis. Thus, by integrating fewer or more data points along the

139 scan pathway, the measurement precision can be adjusted.

140

2.3. Samples

141

142 Fast to slow growing stalagmites and biogenic carbonates (corals, shells) were used in this study (Table 1).

143 Samples were selected according to their (i) ^{14}C signal sequence, i.e. whether they exhibit a distinct signal

144 such as the bomb peak, (ii) the magnitude of the signal rise, and (iii) the spatial expansion of the signal in

145 the sample (detailed information can be found in the SI).

146 *Table 1 Overview of the different samples and sample materials as well as their expected and LA-AMS derived F^{14}C (fraction*

147 *modern).*

Sample label	Type of sample	mineral	Growth rate (µm/a)	Known F^{14}C	Measured F^{14}C (LA-AMS, this study)
ER-77	stalagmite	calcite	120	0.88 – 1.19[13]	0.81 – 1.30[a]
BU-4	stalagmite	calcite	30-50	0.88 – 1.00[33]	0.82 - 1.04[a]
SOP-20	stalagmite	calcite	3-15		0.03 – 0.77[a]
BS_1299m	coral	calcite	35-75	0.92 – 0.98[34]	0.90 – 1.00[a]
Oyster PH3-A	mollusk	aragonite		1.11 – 1.15*	1.09 – 1.22[b]
Arctica islandica	mollusk	aragonite		0.925±0.002*	0.88 – 0.92[b]

148 *this work; [a]normalized to OxII, [b]normalized to CSTD

149

3. Results and Discussion

3.1.Applying the three scanning modes

152 Stalagmite ER-77 was considered "ideal" for comparing the scanning modes due to its distinct ^{14}C profile

153 and high growth rate (120 µm/a). It exhibits a pronounced ^{14}C bomb-peak with an F^{14}C increase of 0.3

154 within several mm. Conventional sampling had been performed at the center of the stalagmite's growth

155 axis with a spatial resolution of 0.6 mm per subsample [13]. The bomb peak expands across the six topmost

156 samples covering a width of ca. 4 mm (Figure 3). The three LA-AMS scanning modes were performed with

157 different offsets to the growth axis: the precision scan (Mode 3) was placed closest to the growth axis

158 covering an effective distance of 3 mm. Discrete layer analysis (Mode 1) covering 4 mm and the survey

159 scan (Mode 2) covering 2.5 mm were performed with increasing distance from the growth axis (detailed

160 information can be found in the SI).

3.1.1. Discrete layer analyses (Mode 1)

162 Nine discrete scans were made, each covering a length of 2–2.6 mm. The scan velocity was set between

163 2.5 and 5 µm/s and the spacing between the individual scans covered 300 µm for the seven topmost

164   samples and 1 mm for the two lower ones. The $^{14}C/^{12}C$ raw data (blue dots) of the nine sub-scans are

165   depicted in Figure 3 a, with the onset of the bomb peak found within 60 minutes of analysis. Horizontal

166   red bars indicate the lifetime of a sputter target and represent the period of continuous data acquisition.

167   The vertical dashed and horizontal black lines represent the "data integration period", which is equal to

168   the "data acquisition period" in the case of "Mode 1." Integrated, background corrected and normalized

169   data are depicted in Figure 3 b, where red circles represent the LA-data and black squares the conventional

170   measurements. For LA-AMS a measurement precision on the order of 2% is achieved corresponding to the

171   uncertainty from counting statistics and the spatial resolution, defined by the crater width, is 110 μm. The

172   material consumption lies between 1 – 1.5 mg per subsample and the measurement time per aliquot

173   ranges from 8 – 15 min, resulting in ca. 2 hours total analysis time. The LA-derived data match the

174   conventionally derived $F^{14}C$ values very well and within the statistical uncertainties, as confirmed by a χ^2-

175   test (95% confidence limit). Since the spacing between individual scans was not minimal, there is capacity

176   for placing two to three additional subsamples between the topmost seven samples and up to nine

177   between the two lower ones.

178

179   ### 3.1.2. Survey scan (Mode 2)

180   A survey scan across the top 2.5 mm of the stalagmite was performed with a scan velocity of 2.5 μm/s

181   resulting in an overall measurement time of 17 minutes. The $^{14}C/^{12}C$ ratios are shown as blue dots in Figure

182   3 c. The scan was performed on one sputter target and data integrated for 60 sec, or a span (Δx) of 150

183   μm respectively. The resulting $F^{14}C$ is represented by the red circles in Figure 3 d. The survey scan was

184   performed within less than 20 minutes, yielding a precision on the order of 4% for each aliquot and a

185   spatial resolution of ca. 260 μm. 1.6 mg of $CaCO_3$ were consumed for the entire scan corresponding to

186   0.1 mg per integration period. A χ^2-test was performed to test the agreement between LA and

187   conventional data within a 95% confidence limit. When the LA-data is shifted by a $F^{14}C$ 0.03 to higher

188   values, the χ^2-test yields good agreement between the two data sets. This offset of the data is discussed

189   in Section 3.3. The LA-scan was performed with an offset of approximately ca. 1 cm relative to the

190   stalagmite growth axis. The growth layer structure at this region is different to that at the center of the

191   stalagmite as growth layers thin out and start to slope with increasing distance from the center. Thus, the

192   bomb peak is found in the upper 2.5 mm instead of the upper 4 mm, as found with conventional analysis,

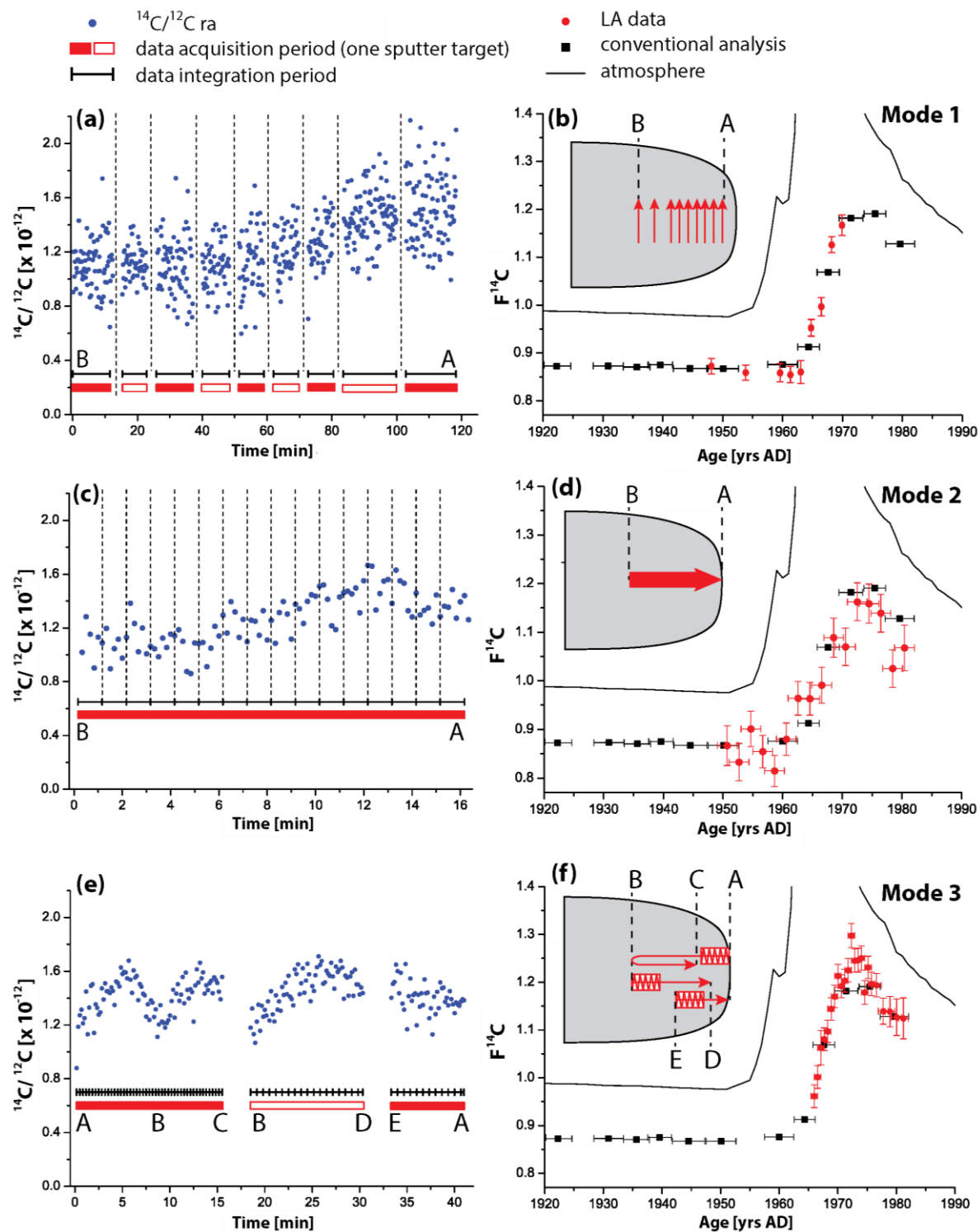193   where samples were taken at the stalagmite's growth axis.

Figure 3 Comparison of the three measurement modes using stalagmite ER-77: (a) and (b) discrete layer analyses, (c) and (d) survey scan, (e) and (f) precision scan. In the left part of the figure corrected $^{14}C/^{12}C$-ratios are plotted against the acquisition time. Red bars (open and solid) correspond to one sputter target and black bars/vertical dashed lines to the integration time. In the right part of the figure, the integrated $F^{14}C$ values are shown and the inserts indicate the path of the scan (not to scale).

195 ### 3.1.3. Precision scan (Mode 3)

196 Three precision scans were performed within the top 3 mm of stalagmite ER-77. The velocity was set to
197 200 µm/s for the first scan, allowing scanning back and forth while using a single sputter target. The scan
198 parameters were Δx = 3 mm, Δy = 2 mm, δx = 100 µm. A second and third scan stacked on the track of the
199 first one, this time facing towards the top, were performed with a scan velocity of 100 µm/s, while all other
200 parameters were kept constant. The scanning paths are shown in the inset of Figure 3 (f) and are reflected
201 in the ^{14}C/^{12}C raw data (blue circles in Figure 3 e). The two peaks on the first sputter target correspond to
202 the back and forth movement across the bomb peak in the sample. The second and third scan were
203 performed with two sputter targets. They overlap at the transition and the bomb peak was crossed only
204 once. The integration time is 60 s, which equals the duration of one zig-zag step (compare black horizontal
205 bars in Figure 3 e) and corresponds to a material consumption of 130 µg CaCO$_3$. The average F^{14}C of the
206 three scans was calculated (red squares in Figure 3 f) and, since the signal intensity at the top of the sample
207 was much lower than for the other samples, the mean of two zig-zag steps was taken for the topmost four
208 data points. The spatial resolution is 300 µm compared to 200 µm achieved for the other subsamples. A
209 measurement precision on the order of 2% is obtained, except for the four data points at the top, for which
210 4% was achieved. The overall measurement time was 40 minutes.

211

212 ### 3.1.4. Comparison of the three LA-AMS scanning modes

213 Each of the presented scanning modes has certain strengths with regard to measurement time, achievable
214 precision, spatial resolution and sample consumption. Spatial resolution and measurement precision
215 depend on the scan velocity, laser parameters and the efficiency of the setup. The major advantage of the
216 three measurement modes, when compared to conventional methods, is the shorter analysis time, and
217 thus sample throughput. This is especially true for the survey scan (Mode 2), which allows analyzing a
218 comparably large section of the sample (i.e., several centimeters within one hour). A quick overview of the
219 ^{14}C-content across a carbonate record can be established using Mode 2 and subsequently a precision scan
220 (Mode 3) at selected regions can be performed to achieve higher measurement precisions. Ablating across
221 different growth layers is only desired in the case of survey scans. For discrete layer analysis (Mode 1) and
222 precision scans (Mode 3) material is collected within individual growth layers. Since the laser beam is a
223 rectangular shape, the maximum scanning distance within each growth layer is limited by the region of
224 parallel growth in the sample and with respect to the laser spot geometry. This could be improved by using
225 a smaller, quadratic or circular laser spot at the expense of CO$_2$ production. To achieve higher precision at

226 a smaller spot size, signal intensities obtained with the LA-AMS setup need to be improved and is the
227 subject of future studies.

228 With the three measurement modes, the ^{14}C signal in stalagmite ER-77 was reproduced within the
229 statistical uncertainties. The precision scan revealed that bomb ^{14}C reaches F^{14}C levels of up to 1.30,
230 whereas conventional data suggested that the peak was at approximately 1.20. This highlights the
231 enormous potential of this novel method because of the increased resolution. The key findings for all three
232 LA-AMS scanning modes and the conventional AMS measurements are summarized in Table 2.

233

234

235 *Table 2 Comparison of the three LA-measurement modes with conventional graphite-AMS measurements of ER-77.*

Measurement mode	time/data point (min)	spatial resolution (µm)	material consumption (mg CaCO$_3$)	measurement precision (%)
micromill and conventional graphite	60	≥ 400	8	0.4
LA – discrete layer	10	100 – 200	1 – 1.5	1 – 2
LA - survey scan	0.5 – 2	300 – 1700	0.1 – 0.2	4 – 6
LA – precision scan	0.5 – 4	200 – 1000	0.1 – 0.4	2 – 4

236

237 ## 3.2. Potential of LA-AMS for stalagmites, corals and other marine carbonates

238 LA-AMS analysis bears enormous potential for the analysis of carbonate archives. Reconnaissance
239 scanning allows rapid identification of the potential of a given sample, thus reducing analysis time and
240 effective costs. In many cases, the ^{14}C–variability is not as pronounced as observed in stalagmite ER-77. In
241 the following section, the potential of the LA-AMS setup for samples with smaller variations in their ^{14}C
242 content, as well as for other carbonate materials is addressed. First, a slow growing stalagmite will be
243 investigated that exhibits an attenuated bomb peak. Second, a stalagmite record is analyzed that exhibits
244 a growth interruption of more than 350 ka. Finally, the LA-AMS setup will be used to investigate a deep-
245 sea coral sample exhibiting a bomb ^{14}C peak, and its potential for use on aragonite shell samples.

246

247

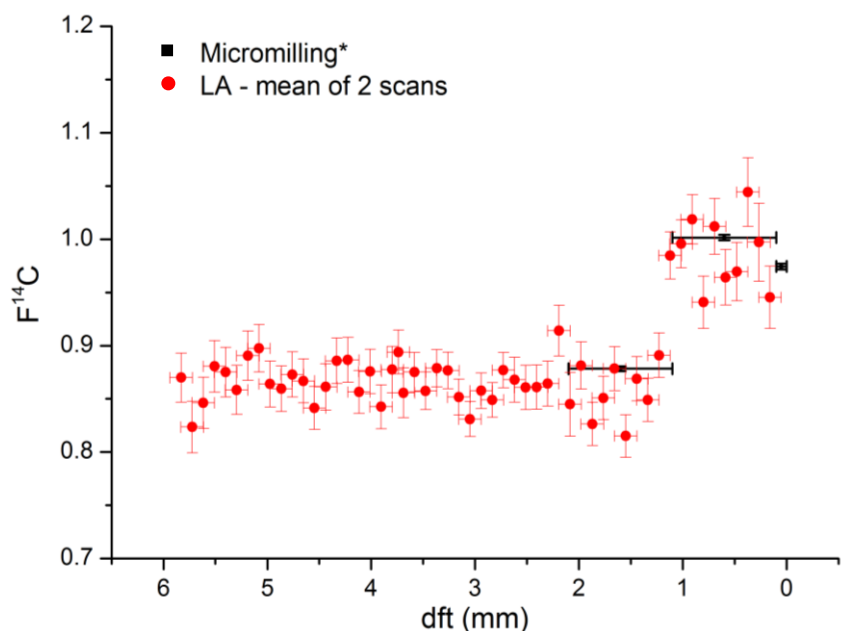248   ## 3.2.1. Attenuated bomb ^{14}C peak in a stalagmite (BU-4)

Figure 4 LA-AMS data (red circles) compared to conventionally derived solid AMS measurements (black squares). The high resolution achieved with LA-AMS allows identification of the abrupt onset of the bomb peak in the upper-most mm of the stalagmite sample.

249

250   Two precision scans were performed in opposite directions within the top 6 mm of the slow growing

251   stalagmite BU-4. Conventionally obtained and LA-AMS derived data match well within the statistical

252   uncertainties (Figure 4). The abrupt onset of the bomb peak was revealed, even though it covered a $F^{14}C$

253   rise of only 0.12 and is located within the uppermost millimeter of the stalagmite (detailed information

254   can be found in the SI). A χ^2 test was performed confirming that the LA and conventional data are not

255   significantly different (95% confidence limit).

256

257   ## 3.2.2. Growth interruption in a stalagmite (SOP-20)

258   Scans in Mode 2 and 3 were performed on all three sections of the Siberian sample. The results for the

259   upper sections can be found in the SI. Two survey scans facing in opposite direction were performed on

260   SOP-20-bottom. Both scans exhibit a clear step in $F^{14}C$ caused by a growth interruption at approximately

261   55 to 56 mm (Figure 5). Assuming an ideal step between the ^{14}C-dead (> 55.5 mm, see Section 1c in SI for

262   details) and ^{14}C-containing (<55.5 mm) sections, carry-over effects and washout of the laser system can be

263   studied. Based on the comparison of both scans, a washout time of approximately 10 sec was estimated.

264
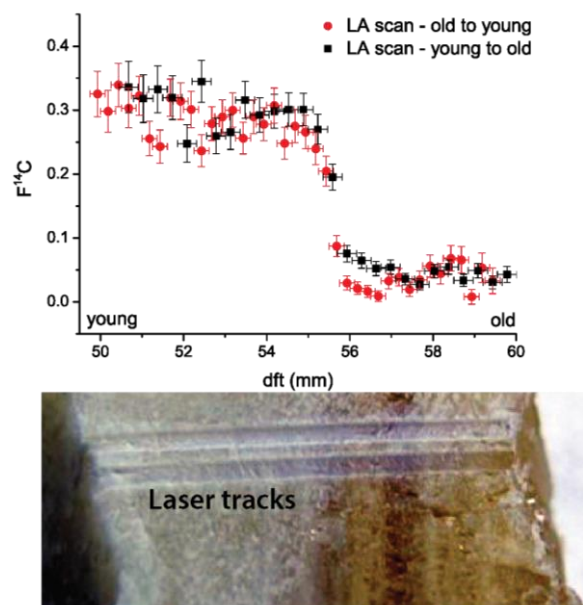
265

266 *Figure 5 Two survey scans were performed on the bottom part of stalagmite SOP-20 confirming the growth interruption identified*
267 *by U-Th ages of 8.711 ± 0.012 ka BP and 377 ± 7 ka BP. (DFT: distance from top).*

268

3.2.3. Other samples

270 To further exemplify the potential of the new LA-AMS method, a calcitic bamboo coral (*Keratoisis* sp.
271 sample BS_1299m[34]) was analyzed using the precision scan (Mode 3). At the outer edge of the sample the
272 bomb peak with an $F^{14}C$ increase of 0.06 was found, which is in agreement with the conventional data
273 (compare Section 2 c and Figure 4 in SI).

274 Two stacked precision scans were performed in opposite directions on a sectioned shell from a black-lip
275 pearl oyster (*Pinctada margaritifera*) from the Hawaiian Islands. Comparison of LA-AMS and conventional
276 ^{14}C data from a series of micromill extractions (both within the shell and from a regional hermatypic coral
277 record) showed good agreement within the statistical uncertainties (compare Section 2 d and Figure 5 in
278 SI).

279 One survey scan was performed on another shell sample from a long-lived species, *Arctica islandica,* found
280 on the beach of Fur, Denmark. Within the topmost 30 mm a $F^{14}C$ of 0.92 ± 0.01 was measured, while the
281 average value of the older part was lower with an $F^{14}C$ value of 0.88 ± 0.02. The LA-data was confirmed by
282 one conventional graphite sample that was in agreement. The sample was taken at the youngest part of
283 the shell and yielded a $F^{14}C$ of 0.925 ± 0.002. In contrast to the initial assumption that this shell contained

284 the bomb peak, the LA-AMS analyses revealed within less than one hour, that the shell was much older

285 (compare Section 2 e and Figure 6 in SI).

286

287 ### 3.3.Potential and limits of LA-AMS

288 The applicability of the novel LA-AMS technique for ^{14}C analyses of various carbonate archives and its

289 potential with regard to spatial resolution and measurement precision has been exemplified with the

290 above described samples. Signal intensities obtained for aragonite and calcite samples were on the same

291 order of magnitude and comparable to ion currents reached for conventional gas measurements. The

292 major advantages of the novel technique are short measurement times and its high spatial resolution. LA-

293 AMS is especially useful for the rapid identification of pronounced ^{14}C signatures, such as the ^{14}C bomb

294 peak or a growth interruption. A major drawback is the measurement precision, which is worsened by a

295 factor of two or even higher compared with conventional graphite analyses. χ^2 tests were performed to

296 confirm the agreement between LA-derived F^{14}C data of samples with conventional data. For samples

297 where external standard gas was used for calibration (compare Table 1), the χ^2 test verified the compliance

298 either directly, or after applying an F^{14}C offset correction between 0.02 – 0.03. The offset is most likely

299 caused by the calibration method, because in this case a standard gas was used, which is introduced into

300 the AMS directly from the gas cylinder. It is still a matter of investigation to identify the origin of the offset.

301 One sample was normalized using the LA-AMS standard CSTD. Even though, the LA-derived data reflects

302 the trend of the conventional data, in this case, the χ^2 test did not confirm that LA-derived and

303 conventional data matched within the 95% confidence interval, not even after performing offset

304 corrections. During the analyses of this sample, exceptionally high background on ^{14}C caused by broken up

305 molecules was observed (see Section 2 c in SI), which is most likely the reason for the discrepancy between

306 LA.

307 For each analyzed sample, the ^{14}C range obtained by LA-AMS was larger than in the case of the

308 conventional analyses (Table 1). Due to the higher spatial resolution achieved with LA-AMS, more detailed

309 insight in the ^{14}C-content within the carbonate record can be gained.

310

311 # 4. Conclusion

312 The LA-AMS technique was successfully applied to ^{14}C analyses of carbonate archives including stalagmites,

313 deep-sea coral and mollusk shells. Different sampling strategies were compared with regard to

314   measurement precision, spatial resolution, analysis time and material consumption. LA-AMS samples

315   required between 0.05 to 1.5 mg of $CaCO_3$ with measurement times ranging from 1 to 10 minutes,

316   whereby a precision of 1 to 6 % and a spatial resolution between 100 and 1700 μm were reached. The

317   different scanning modes complement each other and can be combined in order to yield optimal results

318   which may depend on the focus of the study. Continuous scanning provides great flexibility with regard to

319   measurement precision and spatial resolution. Studies with a limited amount of sample can profit from

320   this new technique because comparably only a small amount of material is consumed. A major advantage

321   of LA-AMS is the exceptional sample throughput that allows a rapid assessment of ^{14}C content on a large

322   number of subsamples. Nevertheless, it is desirable to further increase the measurement precision in

323   order to resolve less pronounced ^{14}C signals. Improving the overall efficiency with a modified LA-cell design

324   and an optimized optical setup would allow for a reduction of the scanning velocity, which would increase

325   the analysis time and consequently improve the counting statistics to close the gap in measurement

326   precision between analysis using LA-AMS compared to conventional gas and graphite analysis. A

327   modification of the cell design and the beam transportation system would also provide an opportunity to

328   operate at higher laser fluences. These improvements of the LA-AMS technique will allow establishing [14]C

329   profiles of carbonate archives with high precision and unprecedented spatial resolution at an exceptionally

330   high sample throughput.

331

Acknowledgements

337

338

339 (1) Mangini, A.; Lomitschka, M.; Eichstadter, R.; Frank, N.; Vogler, S.; Bonani, G.; Hajdas, I.; Patzold, J.
340 *Nature* **1998**, *392*, 347-348.
341 (2) Fleitmann, D.; Burns, S. J.; Mudelsee, M.; Neff, U.; Kramers, J.; Mangini, A.; Matter, A. *Science* **2003**,
342 *300*, 1737-1739.
343 (3) Reimer, P. J.; Baillie, M. G. L.; Bard, E.; Bayliss, A.; Beck, W.; Bertrand, C. J. H.; Blackwell, P. G.; Buck, C.
344 E.; Burr, G. S.; Cutler, K. B.; Damon, P. E.; Edwards, R. L.; Fairbanks, R. G.; Friedrich, M.; Guilderson, T. P.;
345 Hogg, A. G.; Hughen, K. A.; Kromer, B.; McCormac, G.; Manning, S.; Ramsey, C. B.; Reimer, R. W.; Remmele,
346 S.; Southon, J. R.; Stuiver, M.; Talamo, S.; Taylor, F. W.; van der Plicht, J.; Weyhenmeyer, C. E. *Radiocarbon*
347 **2004**, *46*, 1029-1058.
348 (4) Hoffmann, D. L.; Beck, J. W.; Richards, D. A.; Smart, P. L.; Singarayer, J. S.; Ketchmark, T.; Hawkesworth,
349 C. J. *Earth and Planetary Science Letters* **2010**, *289*, 1-10.
350 (5) Ridley, H. E.; Asmerom, Y.; Baldini, J. U. L.; Breitenbach, S. F. M.; Aquino, V. V.; Prufer, K. M.; Culleton,
351 B. J.; Polyak, V.; Lechleitner, F. A.; Kennett, D. J.; Zhang, M. H.; Marwan, N.; Macpherson, C. G.; Baldini, L.
352 M.; Xiao, T. Y.; Peterkin, J. L.; Awe, J.; Haug, G. H. *Nat. Geosci.* **2015**, *8*, 195-200.
353 (6) Druffel, E. R.; Griffin, M. S.; Beaupre, S. R.; Dunbar, R. B. *Geophys. Res. Lett.* **2007**, *34*, L09601.
354 (7) Robinson, L. F.; Adkins, J. F.; Keigwin, L. D.; Southon, J.; Fernandez, D. P.; Wang, S. L.; Scheirer, D. S.
355 *Science* **2005**, *310(5753)*, 1469–1473.
356 (8) Andrews, A. H.; Barnett, B. K.; Allman, R. J.; Moyer, R. P.; Trowbridge, H. D. *Can. J. Fish. Aquat. Sci.* **2013**,
357 *70*, 1131-1140.
358 (9) Scholz, D.; Hoffmann, D. *Quater. Sci. J.* **2008**, *57*, 52-77.
359 (10) Edwards, R. L.; Gallup, C. D.; Cheng, H. *Uranium-Series Geochemistry* **2003**, *52*, 363-405.
360 (11) Rudzka-Phillips, D.; McDermott, F.; Jackson, A.; Fleitmann, D. *Geochimica et Cosmochimica Acta* **2013**,
361 *112*, 32-51.
362 (12) Genty, D.; Vokal, B.; Obelic, B.; Massault, M. *Earth Planet. Sci. Lett.* **1998**, *160*, 795–809.
363 (13) Fohlmeister, J.; Kromer, B.; Mangini, A. *Radiocarbon* **2011**, *53*, 99-115.
364 (14) Adkins, J. F.; Cheng, H.; Boyle, E. A.; Druffel, E. R. M.; Edwards, R. L. *Science* **1998**, *280*, 725-728.
365 (15) Frank, N.; Paterne, M.; Ayliffe, L.; van Weering, T.; Henriet, J. P.; Blamart, D. *Earth Planet. Sci. Lett.*
366 **2004**, *219*, 297-309.
367 (16) Hodge, E.; McDonald, J.; Fischer, M.; Redwood, D.; Hua, Q.; Levchenko, V.; Drysdale, R.; Waring, C.;
368 Fink, D. *Radiocarbon* **2011**, *53*, 345-357.
369 (17) Hua, Q.; McDonald, J.; Redwood, D.; Drysdale, R.; Lee, S.; Fallon, S.; Hellstrom, J. *Quat. Geochronol.*
370 **2012**, *14*, 67-80.
371 (18) Noronha, A. L.; Johnson, K. R.; Southon, J. R.; Hu, C. Y.; Ruan, J. Y.; McCabe-Glynn, S. *Quaternary*
372 *Science Reviews* **2015**, *127*, 37-47.
373 (19) Gray, A. L. *Analyst* **1985**, *110*, 551-556.
374 (20) Pisonero, J.; Fernandez, B.; Guenther, D. *Journal of Analytical Atomic Spectrometry* **2009**, *24*, 1145-
375 1160.
376 (21) Koch, J.; Guenther, D. *Applied Spectroscopy* **2011**, *65*, 155A-162A.
377 (22) Rosenheim, B. E.; Thorrold, S. R.; Roberts, M. L. *Rapid Communications in Mass Spectrometry* **2008**,
378 *22*, 3443-3449.
379 (23) Ruff, M.; Wacker, L.; Gaeggeler, H. W.; Suter, M.; Synal, H. A.; Szidat, S. *Radiocarbon* **2007**, *49*, 307-
380 314.
381 (24) Fahrni, S. M.; Wacker, L.; Synal, H. A.; Szidat, S. *Nuclear Instruments & Methods in Physics Research*
382 *Section B-Beam Interactions with Materials and Atoms* **2013**, *294*, 320-327.
383 (25) Wacker, L.; Muensterer, C.; Hattendorf, B.; Christl, M.; Guenther, D.; Synal, H. A. *Nuclear Instruments*
384 *& Methods in Physics Research Section B-Beam Interactions with Materials and Atoms* **2013**, *294*, 287-290.

385 (26) Münsterer, C.; Wacker, L.; Hattendorf, B.; Christl, M.; Koch, J.; Dietiker, R.; Synal, H. A.; Guntherk, D.
386 *Chimia* **2014**, *68*, 215-216.
387 (27) Welte, C.; Wacker, L.; Hattendorf, B.; Christl, M.; Koch, J.; Synal, H. A.; Günther, D. *Radiocarbon* **2016**
388 **(in press)**.
389 (28) Synal, H. A.; Stocker, M.; Suter, M. *Nuclear Instruments & Methods in Physics Research Section B-Beam*
390 *Interactions with Materials and Atoms* **2007**, *259*, 7-13.
391 (29) Wacker, L.; Bonani, G.; Friedrich, M.; Hajdas, I.; Kromer, B.; Nemec, M.; Ruff, M.; Suter, M.; Synal, H.
392 A.; Vockenhuber, C. *Radiocarbon* **2010**, *52*, 252-262.
393 (30) Wacker, L.; Christl, M.; Synal, H. A. *Nuclear Instruments & Methods in Physics Research Section B-*
394 *Beam Interactions with Materials and Atoms* **2010**, *268*, 976-979.
395 (31) Reimer, P. J.; Brown, T. A.; Reimer, R. W. *Radiocarbon* **2004**, *46*, 1299-1304.
396 (32) Gao, P.; Xu, X.; Zhou, L.; Pack, M. A.; Griffin, S.; Santos, G. M.; Southon, J. R.; Liu, K. *Limnol. Oceanogr.*
397 *Meth.* **2014**, *12*, 174-190.
398 (33) Fohlmeister, J.; Schroeder-Ritzrau, A.; Scholz, D.; Spoetl, C.; Riechelmann, D. F. C.; Mudelsee, M.;
399 Wackerbarth, A.; Gerdes, A.; Riechelmann, S.; Immenhauser, A.; Richter, D. K.; Mangini, A. *Climate of the*
400 *Past* **2012**, *8*, 1751-1764.
401 (34) Farmer, J. R.; Robinson, L. F.; Honisch, B. *Deep-Sea Research Part I-Oceanographic Research Papers*
402 **2015**, *105*, 26-40.

403

404